Photodiagnosis and Photodynamic Therapy 22 (2018) 191–196

Contents lists available at ScienceDirect

Photodiagnosis and Photodynamic Therapy

journal homepage: www.elsevier.com/locate/pdpdt

Photodynamic inactivation assisted by localized surface plasmon resonance of silver nanoparticles: In vitro evaluation on *Escherichia coli* and *Streptococcus mutans*

Martha S. Ribeiro[a], Luciana S.A. de Melo[b], Sajid Farooq[b], Alessandra Baptista[a], Ilka T. Kato[d], Silvia C. Núñez[c], Renato E. de Araujo[b,*]

[a] Center for Lasers and Applications, IPEN-CNEN/SP, 05508-000, São Paulo, SP, Brazil
[b] Laboratory of Biomedical Optics and Imaging, Federal University of Pernambuco, Recife, PE, 50740-530, Brazil
[c] Biomedical Engineering Post-Graduation Program, Universidade Brasil, São Paulo, SP, Brazil
[d] The Engineering, Modelling and Applied Social Science Department, UFABC, 09210-580, Santo André, SP, Brazil

ARTICLE INFO

Keywords:
Metallic nanoparticle
Bacterial inactivation
Photosensitizer uptake
Antimicrobial
Blue LED

ABSTRACT

Localized surface plasmon resonance (LSPR) of gold nanoparticles has been reported to increase the antimicrobial effect of the photodynamic therapy. Although silver nanoparticles (AgNPs) are an efficient growth inhibitor of microorganisms, no studies exploring LSPR of AgNPs to enhance the photodynamic inactivation (PDI) have been related. In this work, we described the LSPR phenomenon of AgNP sand investigated its interaction with riboflavin, a natural photosensitizer. We evaluated the use of AgNPs coated with pectin (p-AgNP) in riboflavin (Rb)-mediated PDI of *Escherichia coli* (Gram- bacteria) and *Streptococcus mutans* (Gram + bacteria) using a blue light-emitting diode ($\lambda = 455 \pm 20$ nm) of optical power 200 mW. Irradiance was 90 mW/cm^2 and radiant exposure varied according to the time exposure. Uptake of Rb and p-AgNP by the cells was evaluated by measuring the supernatant absorption spectra of the samples. We observed that LSPR of p-AgNPs was able to enhance the riboflavin photodynamic action on *S. mutans* but not on *E. coli*, probably due to the lower uptake of Rb by *E. coli*. Taken together, our results provide insights to explore the use of the LPRS promoted by silver nanostructures to optimize antimicrobial PDI protocols.

1. Introduction

Light-based therapy and diagnosis are essential non-invasive tools for medical and biomedical applications. The interaction of light with biological tissue can be prompted with the use of external agents, as photosensitizers, dyes, scatters, and fluorescent particles [1,2]. In particular, photodynamic inactivation (PDI) has been extensively used as a promising antimicrobial approach since it does not promote the selection of mutant resistant strains [3,4]. PDI explores the light-interaction with specific photosensitizers (PSs) to induce oxidative stress on microorganism, leading to cell death via different targets [5,6].

More recently, metallic nanoparticles (NPs) have been also manipulated on the development of new biomedical sensor [7], contrast agents [8], and to improve light-based therapies [9–11]. Biomedical applications of metallic NPs are driven by the interaction of light with nanostructure that leads to a collective resonance of the conduction electrons in the metal, known as Localized Surface Plasmon Resonance (LSPR) effect [12]. At resonance, metallic NPs can scatter light with remarkable efficiency, enhancing the electric field density close to the metal surface. The NP material, size, shape and surrounding medium determine the magnitude and resonance frequency of LSPR effect [13]. Also, the field density boost can be sensed by molecules that are placed close to the NP, and therefore inducing, for instance, a luminescence enhancement.

To establish NP LSPR-PS interaction it is required that LSPR frequency and the PS absorption spectrum overlap. Thus, the PS could perceive the field enhancement close to the NP surface, and a better excitation of the PS molecule could be promoted [14]. In fact, spherical AgNPs present a LSPR peak at the blue region of the electromagnetic spectrum [15] and since some PSs can be excited using blue light, as porphyrins and riboflavin, singlet oxygen ($^1O_2$) generation by PSs could be enhanced by LSPR of AgNP [16].

Zhang et al. were the first to demonstrate that LSPR may induce singlet $^1O_2$ generation enhancement by displacing PSs on a non-continuous silver film [17]. Melo and coworkers also observed metal-enhanced singlet oxygen (MEO) generation in riboflavin (Rb) water

* Corresponding author.
E-mail address: renato.earaujo@ufpe.br (R.E. de Araujo).

https://doi.org/10.1016/j.pdpdt.2018.04.007
Received 23 August 2017; Received in revised form 11 April 2018; Accepted 13 April 2018
Available online 17 April 2018

solution with silver-pectin nanoparticles [16]. In that work, pectin, a complex carbohydrate found in plants primary cell walls, was used to improve 28.5% MEO generation by Rb.

The use of PDI assisted by LSPR using gold NPs conjugated to different PSs has been described in literature [18–20]. Khan et al. showed significant reduction of *Candida albicans* biofilm using PDI mediated by AuNP-methylene blue conjugate [18]. Other authors suggest that AuNP could be employed in the photodynamic treatment of cutaneous *C. albicans* infections [19] or to treat a Crohn's disease-associated *Escherichia coli* [20]. In contrast, AgNP-mediated PDI using LSPR has been little explored. In Nombona et al. study, authors reported efficient PDI of *Staphylococcus aureus* due to Zn phthalocyanine-polylysine conjugated to gold and silver nanoparticles [21]. In their work, the use of silver showed to be more effective than gold nanostructures.

In fact, a higher electromagnetic field enhancement can be obtained by LSPR in silver than in gold nanoparticles [22,23]. Therefore, with a proper PS, silver NPs could enhance PDI action on microorganism. Moreover, as silver is commonly used in therapeutics because its antimicrobial activity, the use of AgNPs could be more attractive for bactericidal purpose [24]. Thus, in this work, we describe the LSPR effect of AgNPs coated with pectin (p-AgNP) and investigate its interaction with Rb, also known as B2 vitamin, a natural PS. Thereafter, we exploit the effects of LSPR-mediated PDI on *Escherichia coli* and *Streptococcus mutans,* a Gram- and a Gram + bacterium, respectively.

2. Theoretical development

2.1. Localized surface plasmon resonance

The coupling phenomenon of electromagnetic field of incident light with conduction electrons of metal nanoparticles, as Au and Ag, is characterized by a unique extinction spectrum. When the size of noble metal nanoparticle is much smaller than the light wavelength, a quasi-static approximation can be used to analyze the NP scattering, absorption and extinction cross-section. Moreover, light interaction with a small sphere having sub-wavelength radius, b, can be described by the polarizability, α, defined as [25]:

$$\alpha = 4\pi b^3 \left(\frac{\varepsilon - \varepsilon_m}{\varepsilon + 2\varepsilon_m}\right), \tag{1}$$

where ε is the frequency-dependentcomplex permittivity of the spherical particle, i.e., $\varepsilon(\omega) = \varepsilon_r(\omega) + \varepsilon_i(\omega)$, and ε_m is the permittivity of the surrounding medium. Eq. (1) indicates that, for a non-absorbent medium, polarizability value is maximum when $Re(\varepsilon) = -2\varepsilon_m$, known as Fröhlich condition. At Fröhlich condition, the electric field interaction with the nanoparticle is enhanced, and the plasmon resonance is established.

Using quasi-static limit, the scattering and absorption cross-section (C_{sca} and C_{abs}) can be attributed to the polarizability, as $C_{sca.} = \frac{k^4}{6\pi}|\alpha|^2$ and $C_{abs.} = kIm(\alpha)$, where $k = \frac{2\pi}{\lambda}$ is the incident light wavenumber, and $Im(\alpha)$ indicates the imaginary component of the polarizability. The scattering (absorption) cross-section is defined as the ratio of the total radiant power scattered (absorbed) by a particle, to the radiant power incident on the particle.

By using Eq. (1), the scattering cross-section of a spherical particle is given by

$$C_{sca} = 8\pi\frac{k^4}{3}b^6\left|\frac{\varepsilon - \varepsilon_m}{\varepsilon + 2\varepsilon_m}\right|^2 \tag{2}$$

and absorption cross-section can be written as

$$C_{abs} = kIm(\alpha) = 4\pi k b^3 Im\left(\frac{\varepsilon - \varepsilon_m}{\varepsilon + 2\varepsilon_m}\right) \tag{3}$$

For particles with $b << \lambda$, the efficiency of absorption (proportional to b^3) is much higher than scattering efficiency (proportional to b^6). Moreover, for a sphere with volume V, extinction cross-section, $C_{ext} = C_{sca} + C_{abs}$ is

$$C_{ext} = \frac{9\omega}{c}\varepsilon_m^{1.5} V \frac{\varepsilon_i}{(\varepsilon_r + \varepsilon_m)^2 + (\varepsilon_i)^2}. \tag{4}$$

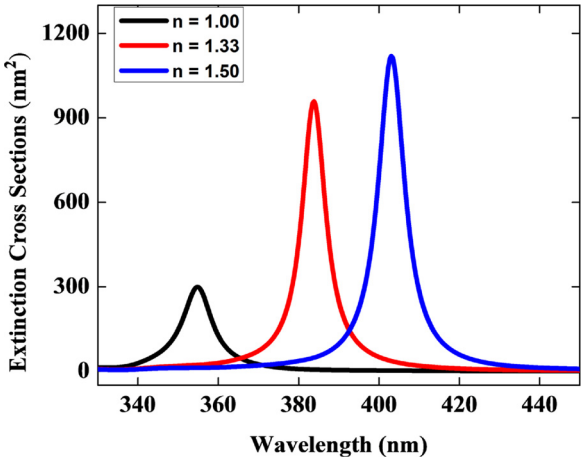

Fig. 1. Extinction cross-section calculated using Eq. (4) for a 10 nm diameter Ag sphere in air (black), water (red) and in pectin (blue).

To determine C_{sca}, C_{abs} and C_{ext} the complex permittivity of the spherical particle should be known. Drude model could be explored to describe the frequency dependence of the particle permittivity. However, Drude model is limited for high energy (blue and UV) photons to describe the real and imaginary part of silver permittivity. High energy photons can induce interband transitions, increasing the damping effect and enhancing the imaginary part of permittivity [26].

Using the real and imaginary parts of permittivity values for silver reported by Johnson and Christy [26] and Eq. (4), the extinction spectrum of 10 nm diameter silver nanospheres was obtained, as shown in Fig. 1. For spheres with diameter smaller than 10 nm, extinction spectrum is mainly determined by absorption process. The peak at the extinction spectrum indicates the establishment of the LSPR condition.

Observe that the extinction cross-section values change with the modification of the surrounding medium permittivity and a red shift of the LSPR peak is obtained (358–404 nm) by increasing the medium refractive index values, from 1.00 (air) to 1.50 (pectin).

LSPR excited in noble metallic NPs such as gold and silver causes strong local field enhancement at the surface of the nanostructures. Fig. 2 shows the electric field enhancement close to a 10 nm diameter AgNP, in a pectin medium, obtained by Finite Element Method (FEM) within Comsol Multiphysics. FEM also was used to calculate frequency-

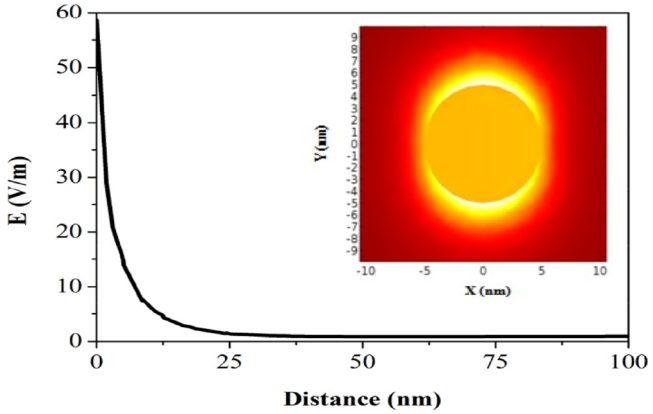

Fig. 2. The electric field distribution with respect to distance from the Ag nanosphere surface in pectin. Inset shows the E-field distribution around the surface of Ag nanosphere at LSPR wavelength.

domain scattering electric field exploring a background oscillating field of arbitrary amplitude ($1\ V\ m^{-1}$). The graphic traced the value of |E| (V/m) versus the distance (nm) from the sphere surface. It is observed that on the surface the amplitude of the field is maximum. The electric field (E-field) decreases as the distance from the surface increases. For distances smaller than 5 nm from the sphere surface, a ~15-fold enhancement is observed. Inset of Fig. 2 depicts the E-field distribution on silver nanosphere surface.

The field decays rapidly from the surface of the NP and vice versa. Therefore, for an efficient MEO, controlling the distance between the PS molecule and the NP can be an important issue. On a solution base platform, PS-NP distance can be established by the electrostatic interaction, by the relative concentration of PS and NPs, or by introducing a shell on the metallic NP surface.

3. Experimental development

3.1. Material and methods

Streptococcus mutans (ATCC 25,175) and *Escherichia coli* (ATCC 33,694) were cultured in brain heart infusion (BHI) broth at 37 °C, under a 5% CO_2 atmosphere for 48 h and 20 h, and used at exponential phase of growth. Cells were harvested by swab and further suspended in either distilled water or 0.9% saline solution. Suspensions of 10^7 colony forming units per milliliter (CFU/ml) were standardized setting the optical density of 0.15 at 540 nm (Spectrophotometer SP220, Biospectro, Brazil) with subsequent dilution at 1:10.

Nanoparticles consisted of silver nanospheres involved by a layer of pectin that were prepared according to Melo et al. [16]. Briefly, one-ml of pectin solution 0.5% w/v (CP Kelco brand, type Genu 105) and 3 ml of 10^{-3} M $AgNO_3$ solution (Sigma-Aldrich, Milwaukee, MI) were added to 25 ml of distilled water. The mixture was heated under stirring and at 80 °C was added 1 ml of sodium citrate 0.1 M (Sigma-Aldrich, Milwaukee, MI). The system was maintained heated (80 °C–100 °C) for 30 min until the formation of a yellowish colloidal suspension. In this way, we obtained 8.3×10^{12}AgNP/ml of 13 ± 4 nm diameter sphere. A stock solution of 133.3μg/ml Rb (Sigma-Aldrich, Milwaukee, MI) was prepared in distilled water.

For PDI assays, bacteria cells were incubated with p-AgNP, riboflavin (Rb) or p-AgNP plus riboflavin (p-AgNP + Rb) solutions for 10 min at room temperature in the dark. Nanoparticles were used at a concentration of 2.49×10^{12} p-AgNP/ml and Rb at 40 μg/ml.

An aliquot of 150 μl was collected from each group, placed on a plate of 96 wells and irradiated with a blue light emitting diode (LED) at λ = 455 ± 20 nm (MMOptics, São Carlos, Brazil). The irradiation parameters were fluence rate of 90 mW/cm^2, exposure time of 2, 4, and 6 min and optical power of 200 mW. All samples used had the same volume. The tip of the LED was placed perpendicular to the wells and irradiation was uniformly performed. Five groups of samples were evaluated: I) **Control**, no irradiation, Rb or p-AgNP; II) **L**, LED illumination in absence of p-AgNP or Rb for 6 min; III) **NP**, p-AgNP with and without illumination; IV) **PS**, Rb with and without illumination; V) **NP + PS**, p-AgNP and Rb with and without illumination.

After treatment, twenty-μl of the suspension were collected and serially diluted in 180 μl of phosphate-buffered saline (PBS) until dilution of 10^{-5} times the original concentration. Ten-μL of each dilution were streaked on BHI plates in triplicate with the aid of a multichannel pipette. Plates were then incubated during 24 h at 37 °C to obtain CFU/ml values. Microbiological assays were performed in three different days.

To evaluate the Rb and p-AgNP uptake by the cells, *E. coli* and *S. mutans* were cultured in brain heart infusion (BHI) agar at 37 °C, under a 5% CO_2 atmosphere for 24 h. Cells were harvested by swab and further suspended in distilled water. Suspensions of 10^7 CFU/ml were standardized setting the optical density of 0.15 at 540 nm (Spectrophotometer SP220, Biospectro, Brazil). After that, bacterial suspensions were incubated for 10 min with p-AgNP, Rb and p-AgNP + Rb at final concentrations of 2.49×10^{12} p-AgNP/ml and 40 μg/ml Rb, respectively. Under these conditions, no bacterial killing was observed. Bacterial cells were centrifuged (4000 *g*) and 200 μl of the supernatant was placed in wells of a 96 well microtiter plate. The cell suspension alone was also used to establish the blank. Absorbance spectra of the samples were obtained in triplicate with a spectrophotometer (SpectraMAX, GeminiEM, Molecular Devices, USA). Unpaired Student's t test was used on the evaluation of the experimental results.

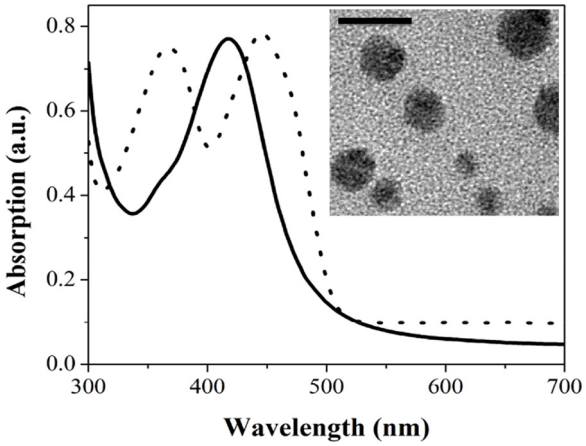

Fig. 3. UV–vis absorbance of colloidal solutions of p-AgNP (continuous line) and of a riboflavin solution (dotted line). Inset: TEM image of p-AgNP (scale bar, 20 nm).

4. Results

Fig. 3 shows that Rb photosensitizer absorption spectrum and the p-AgNP LSPR peak are superposed, indicating that both Rb and p-AgNP could be excited simultaneously by a blue light. Fig. 3 also depicts that the LSPR peak of the p-AgNP is centered at 412 nm, close to value expected from the theoretical value displayed in Fig. 1.

The presence of pectin shell on the nanoparticle surface induces a red shift (4 nm) of the LSPR peak wavelength, as discussed by de Melo et al. [16]. The LSPR wavelength shift prompted by the adhesion of an adsorption layer on a nanoparticle surface can be described by Campbell's model [27]. By exploring Campbell's model and the electric field decay length value (2.34 nm), obtained from Fig. 2, the pectin shell thickness was estimated to be about 1 nm.

The inset of Fig. 3 shows the TEM of the silver nanoparticles. On imaging the p-AgNP, the high energy of the electronic beam from the TEM destroys the pectin coating, limiting the identification of the nanostructure organic shell.

Fig. 4(a) and (b) display, respectively, the survival fraction of *S. mutans* and *E. coli* cells upon treatments. Our results showed that incubation of *S. mutans* or *E. coli* with Rb or p-AgNP alone or p-AgNP and Rb combined, with no illumination, did not cause any cytotoxic effect ($P > 0.05$). Fig. 4 also shows that LED irradiation alone or the combination of p-AgNP and LED irradiation did not significantly affect the viability of both bacteria ($P > 0.05$), indicating that photothermal process was not present.

Illuminating the samples, PDI was observed for the Gram + bacteria. The higher the fluence applied, the higher antimicrobial effect was observed with PDI and PDI associated to p-AgNP. Rb-mediated PDI showed less than 1 log reduction (77.5%) of the viable cells after 6 min of irradiation, whereas the association of p-AgNP to Rb-mediated PDI caused up to 3 log reduction (99.2%) of the bacterial burden (Fig. 4a).

Therefore, p-AgNP was able to enhance the PDI action on *S. mutans*

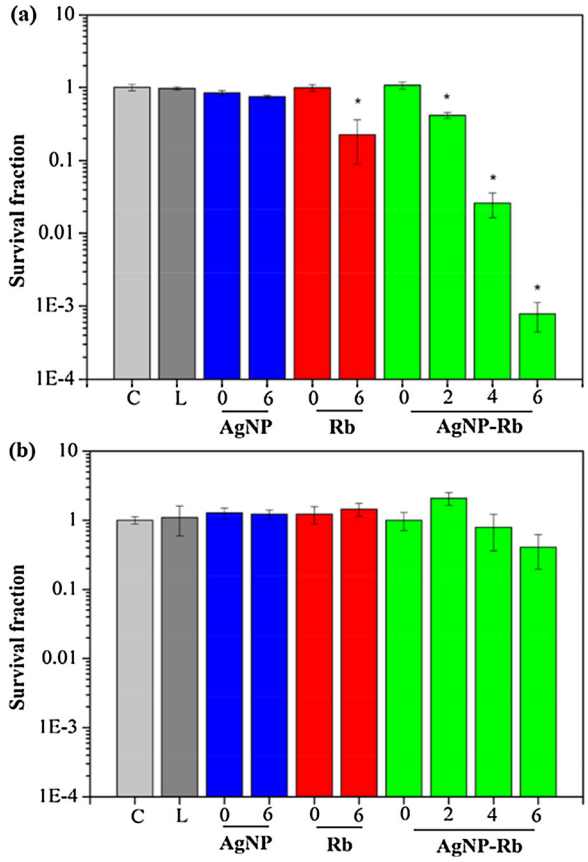

Fig. 4. Mean values ± SD of the survival fraction of *S. mutans* (a) and *E. coli* (b) control and treatment groups. On the x-axis, the numbers from 0 to 6 indicate the irradiation time (in minutes). * represents statistically significant differences compared to control ($p < 0.05$).

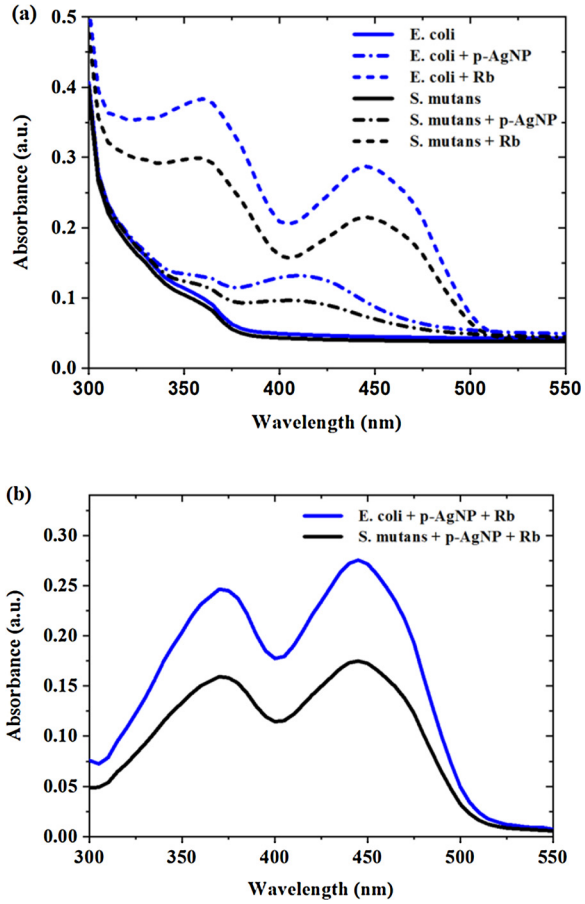

Fig. 5. Mean supernatant absorbance of *S. mutans* and *E. coli* (a) alone, with p-AgNP and with Rb; (b) with p-AgNP + Rb. In (b), the bacterial absorbance was subtracted from the spectra.

but no on *E. coli* (Gram- bacteria)(Fig. 4b). In fact, no statistically significant decrease in bacterial viability was detected for *E. coli*.

Fig. 5a exhibits the supernatant absorption spectra of *S. mutans* and *E. coli*. As shown in Fig. 5a, the microorganisms absorb UV light ($\lambda < 370$ nm). After incubating the bacteria cells with p-AgNP, a peak at 412 nm was observed on the supernatant spectra (*S. mutans* + p-AgNP and *E. coli* + p-AgNP), indicating the presence of the metallic nanoparticle in the supernatant. Fig. 5a also shows the supernatant absorption spectra after incubating the microorganism with Rb (*S. mutans* + Rb and *E. coli* + Rb). Similar to Fig. 3, the peaks at ~445 nm and 360 nm are due to the presence of the PS in the supernatant solution. In Fig. 5b, the supernatant absorption spectra after incubating the bacteria cells with p-AgNp and Rb (*S. mutans* + p-AgNp + Rb and *E. coli* + p-AgNp + Rb) are shown. The bacterial absorbance was subtracted in Fig. 5b. Due to the low concentration of nanoparticle, the supernatant spectra, in Fig. 5b, are mainly determined by the Riboflavin absorption properties. Regardless the evaluated groups (Rb, p-AgNP or Rb + p-AgNP), absorbance peaks for *S. mutans* samples are always significantly lower compared to values obtained from the *E. coli* samples (Table 1), i.e., uptake of Rb and p-AgNP by *S. mutans* in any case is higher than by *E. coli* ($p > 0.05$). In fact, Rb and p-AgNP uptake values were also estimated, as shown in Table 1. The uptake values were obtained by calculating the number of PS molecules and p-AgNP in the supernatant, and subtracting it from the original amount of Rb (40 μg/ml) and nanoparticles (2.49×10^{12} p-AgNP/ml) used on the microorganism samples. The number of PS molecules and p-AgNP in the supernatant is determined by:

$$\left(N_{Rb\ or\ p-AgNp} = \frac{A_{(Rb\ or\ p-AgNP)}}{\varepsilon . l} N_{av} V\right) \quad (5)$$

Table 1
Mean values ± standard deviation of the absorption spectra peak and uptake values of the p-AgNp, Rb and Rb + p-AgNP for *S. mutans* and *E. coli*. The bacteria absorbance values were subtracted from the presented results.

	Absorbance		Uptake (molecule/cell; NP/cell)	
	S. mutans	*E. coli*	*S. mutans*	*E. coli*
p-AgNP*	0.054 ± 0.001	0.084 ± 0.001	8.2×10^5	8.1×10^5
Rb*	0.210 ± 0.001	0.288 ± 0.002	3.4×10^9	2.5×10^9
Rb + p-AgNP*	0.175 ± 0.002	0.275 ± 0.004	–	–

* indicates statistically significant differences between *S. mutans* and *E. coli*.

where A is the absorbance of Rb or p-AgNP obtained from Fig. 5a, ε is the molar extinction coefficient, *l* is the pathlength, N_{Av} is the Avogadro's number, and V is the work volume. The Rb molar extinction coefficient, at $\lambda = 445$ nm, is $\sim 12{,}500\ M^{-1}\,cm^{-1}$, while the p-AgNP extinction coefficient value used was $\sim 10^{-10}\ M^{-1}\,cm^{-1}$, estimated from Fig. 1.

5. Discussion

Metallic nanoparticles have already been manipulated to improve PDI outcome, mainly AuNP [18–20]. On the other hand, LPRS of AgNP to enhance PDI has been little investigated [21].

In this study, we used Rb as photosensitizer because its absorption band matches the absorbance of AgNPs (see Fig. 3). Besides, a plethora

of literature reports efficient bacterial killing following Rb-mediated PDI [28–30]. Rb is able to yield about 50% of $^1O_2$ upon irradiation [31] and enhanced singlet oxygen generation in Rb aqueous solution with p-AgNP has been reported [16].

On metal enhanced oxygen singlet generation, the metallic NP-PS distance is a relevant factor. Thus, particle charge, structure and concentration may play an important rule on LSPR assisted PDI. In a solution, electrostatic interaction can aggregate NP and PS, with the same charge signal, leading to resonance energy transfer (RET) that can reduce the production of $^1O_2$. For compounds with opposite charges, RET can be avoided by controlling the NP–PS distance with the solution compounds concentration. RET effect can also be prevented by using core-shell metallic nanostructure, in which a dielectric shell limits the NP–PS distance. In particular, the presence of a pectin layer on the NP surface can avoid RET, improving the activation of the PS.

Our results showed that Rb-mediated PDI was successful for Gram + bacteria and further bacterial killing was observed combining LPRS of AgNPs while no significant inactivation was noticed for the Gram- bacterium. This finding was unexpected since it is known that AgNPs demonstrate a bactericidal potential [32–34]. AgNP toxicity arises from silver ions released, which affect DNA replication and ATP production or damage cell membranes [35], and is more pronounced in Gram- than Gram + bacteria [33]. Also, Pallavicini et al. showed that p-AgNPs had a high antibacterial activity on *Staphylococcus epidermidis* and *E. coli* [36]. The 24 h minimal inhibitory concentration (MIC) of p-AgNPs against *E. coli* was found to be 31.25 μM, and against *S. epidermidis* the MIC value was 500 μM [36].

Our study was specially designed using a low concentration of p-AgNP (~4 nM) to avoid photothermal effects and to reduce the intrinsic cytotoxicity of the metallic nanostructure, and therefore better identify the MEO action on the bacterial cells. Moreover, the supernatant absorbance values (Table 1) indicate that *E. coli* and *S. mutants* considerably absorbed the metallic nanoparticles. Therefore no significant difference on the NP uptake values was observed. However, PDI enhancement was only observed for Gram + bacteria. This finding matches that reported by Nakonieczna et al., who evaluated the action of 5.5 nm AgNPs and the MIC was 6.74×10^{12} particles/ml with no significant influence on mammalian cell viability with and without illumination. In their work, PDI rendered *S. aureus* (Gram+) more susceptible besides being synergistic to AgNPs [9].

On the other hand, literature reports that Gram+ are more susceptible than Gram- bacteria following PDI, due to the organization of the microorganism outer membrane structures [6,37]. The cell wall of Gram + bacteria contains a thick porous layer of peptidoglycan surrounded by proteins and lipoteichoic acid that allows PS to access through it whilst the cell wall of Gram- bacteria comprises a thin layer of peptidoglycan contiguous to the inner cytoplasmic membrane and an outer membrane with phospholipids and lipopolysaccharides. This outer membrane serves as an obstacle, limiting the PS permeation and binding [38]. Thus, we can also assume that Rb, a neutral PS, was not effective to penetrate the *E. coli* cell wall so that PDI was not able to kill the bacterial cells.

We suggest that the oxidative stress produced by Rb-mediated PDI assisted by LPRS of p-AgNPs was more efficient to damage *S. mutans* because the higher PS uptake, which lead to a higher bacterial burden reduction [39–41]. Although the molar concentration of p-AgNP in this work is much lower than MIC reported by Pallaviciniand coworkers [36], it was enough to allow metal enhanced-PDI for the Gram + bacteria. [35].

Silver cytotoxicity on microorganisms makes AgNPs highly attractive for bactericidal purpose. The use of AgNPs on microorganism control can be expanded exploiting LSPR. Field enhancement around metallic nanoparticles can induce a better excitation of PS molecules and therefore improve the production of highly reactive oxygen species to kill cells. For that, the PS absorption spectrum should overlap the NP plasmon peak. Moreover, the field enhancement around metallic NP may extent up to 10 nm away from the NP surface. Therefore, for an efficient MEO, the PS molecule should remain close to the NP.

Here we evaluated the use of p-AgNP in Rb-mediated PDI on *E. coli* and *S. mutans*, a Gram- and a Gram + bacterium, respectively. We demonstrated enhancement of PDI assisted by LSPR of p-AgNP on *S. mutans* but not on *E. coli*. Our results provide insights to understand the LPRS phenomenon and exploit it to optimize metallic NP-mediated PDI protocols.

Acknowledgements

Authors are grateful to Conselho Nacional de Desenvolvimento Científico e Tecnológico (CNPq), the National Institute of Science and Technology of Photonics (INCT de Fotônica), and the Coordenação de Aperfeiçoamento de Pessoal de Nível Superior (CAPES) for financial supports and student fellowships.

References

[1] R.R. Allison, G.H. Downie, R. Cuenca, X.-H. Hu, C.J. Childs, C.H. Sibata, Photosensitizers in clinical PDT, Photodiagnosis Photodyn. Ther. 1 (2004) 27–42, http://dx.doi.org/10.1016/S1572-1000(04)00007-9.
[2] J.-L. Coll, Cancer optical imaging using fluorescent nanoparticles, Nanomedicine (Lond.). 6 (2011) 7–10, http://dx.doi.org/10.2217/nnm.10.144.
[3] F.F. Sperandio, Y.-Y. Huang, M.R. Hamblin, Antimicrobial photodynamic therapy to kill Gram-negative bacteria, Recent Pat. Antiinfect. Drug Discov. 8 (2013) 108–120 (Accessed 19 July 2017), http://www.ncbi.nlm.nih.gov/pubmed/23550545.
[4] A. Tavares, C.M.B. Carvalho, M.A. Faustino, M.G.P.M.S. Neves, J.P.C. Tomé, A.C. Tomé, J.A.S. Cavaleiro, Â. Cunha, N.C.M. Gomes, E. Alves, A. Almeida, Antimicrobial photodynamic therapy: study of bacterial recovery viability and potential development of resistance after treatment, Mar. Drugs 8 (2010) 91–105, http://dx.doi.org/10.3390/md8010091.
[5] F. Vatansever, W.C.M.A. de Melo, P. Avci, D. Vecchio, M. Sadasivam, A. Gupta, R. Chandran, M. Karimi, N.A. Parizotto, R. Yin, G.P. Tegos, M.R. Hamblin, Antimicrobial strategies centered around reactive oxygen species – bactericidal antibiotics, photodynamic therapy, and beyond, FEMS Microbiol. Rev. 37 (2013) 955–989, http://dx.doi.org/10.1111/1574-6976.12026.
[6] L. Huang, Y. Xuan, Y. Koide, T. Zhiyentayev, M. Tanaka, M.R. Hamblin, Type I and type II mechanisms of antimicrobial photodynamic therapy: an in vitro study on gram-negative and gram-positive bacteria, Lasers Surg. Med. 44 (2012) 490–499, http://dx.doi.org/10.1002/lsm.22045.
[7] A.R. Camara, P.M.P. Gouvêa, A.C.M.S. Dias, A.M.B. Braga, R.F. Dutra, R.E. de Araujo, I.C.S. Carvalho, Dengue immunoassay with an LSPR fiber optic sensor, Opt. Express. 21 (2013) 27023, http://dx.doi.org/10.1364/OE.21.027023.
[8] A.K.S. Braz, R.E. de Araujo, T.Y. Ohulchanskyy, S. Shukla, E.J. Bergey, A.S.L. Gomes, P.N. Prasad, In situ gold nanoparticles formation: contrast agent for dental optical coherence tomography, J. Biomed. Opt. 17 (2012) 66003, http://dx.doi.org/10.1117/1.JBO.17.6.066003.
[9] J. Nakonieczna, A. Rapacka-Zdonczyk, A. Kawiak, K.P. Bielawski, M. Grinholc, Sublethal photodynamic inactivation renders Staphylococcus aureus susceptible to silver nanoparticles, Photochem. Photobiol. Sci. 12 (2013) 1622, http://dx.doi.org/10.1039/c3pp50039j.
[10] L.F. Freitas, M.R. Hamblin, F. Anzengruber, J.R. Perussi, A.O. Ribeiro, V.C.A. Martins, A.M.G. Plepis, Zinc phthalocyanines attached to gold nanorods for simultaneous hyperthermic and photodynamic therapies against melanoma in vitro, J. Photochem. Photobiol. B Biol. 173 (2017) 181–186, http://dx.doi.org/10.1016/j.jphotobiol.2017.05.037.
[11] H. Eshghi, A. Sazgarnia, M. Rahimizadeh, N. Attaran, M. Bakavoli, S. Soudmand, Protoporphyrin IX-gold nanoparticle conjugates as an efficient photosensitizer in cervical cancer therapy, Photodiagnosis Photodyn. Ther. 10 (2013) 304–312, http://dx.doi.org/10.1016/j.pdpdt.2013.02.003.
[12] K.M. Mayer, J.H. Hafner, Localized surface plasmon resonance sensors, Chem. Rev. 111 (2011) 3828–3857, http://dx.doi.org/10.1021/cr100313v.
[13] K.L. Kelly, E. Coronado, L.L. Zhao, G.C. Schatz, The optical properties of metal nanoparticles: the influence of size, shape, and dielectric environment, J. Phys. Chem. B 107 (2003) 668–677, http://dx.doi.org/10.1021/jp026731y.
[14] Y. Zhang, K. Aslan, M.J.R. Previte, C.D. Geddes, Plasmonic engineering of singlet oxygen generation, Proc. Natl. Acad. Sci. U. S. A. 105 (2008) 1798–1802, http://dx.doi.org/10.1073/pnas.0709501105.
[15] L. Wei, J. Lu, H. Xu, A. Patel, Z.S. Chen, G. Chen, Silver nanoparticles: synthesis, properties, and therapeutic applications, Drug Discov. Today 20 (2015) 595–601, http://dx.doi.org/10.1016/j.drudis.2014.11.014.
[16] L.S.A. de Melo, A.S.L. Gomes, S. Saska, K. Nigoghossian, Y. Messaddeq, S.J.L. Ribeiro, R.E. de Araujo, Singlet oxygen generation enhanced by silver-pectin nanoparticles, J. Fluoresc. 22 (2012) 1633–1638, http://dx.doi.org/10.1007/s10895-012-1107-4.
[17] Y. Zhang, K. Aslan, M.J.R. Previte, C.D. Geddes, Metal-enhanced singlet oxygen generation: a consequence of plasmon enhanced triplet yields, J. Fluoresc. 17 (2007) 345–349, http://dx.doi.org/10.1007/s10895-007-0196-y.
[18] S. Khan, F. Alam, A. Azam, A.U. Khan, Gold nanoparticles enhance methylene blue-

induced photodynamic therapy: a novel therapeutic approach to inhibit Candida albicans biofilm, Int. J. Nanomed. 7 (2012) 3245–3257, http://dx.doi.org/10.2147/IJN.S31219.
[19] M.A. Sherwani, S. Tufail, A.A. Khan, M. Owais, Gold nanoparticle-photosensitizer conjugate based photodynamic inactivation of biofilm producing cells: potential for treatment of C. albicans infection in BALB/C mice, PLoS One 10 (2015) e0131684, http://dx.doi.org/10.1371/journal.pone.0131684.
[20] R. Jijie, T. Dumych, L. Chengnan, J. Bouckaert, K. Turcheniuk, C.-H. Hage, L. Heliot, B. Cudennec, N. Dumitrascu, R. Boukherroub, S. Szunerits, Particle-based photodynamic therapy based on indocyanine green modified plasmonic nanostructures for inactivation of a Crohn's disease-associated Escherichia coli strain, J. Mater. Chem. B 4 (2016) 2598–2605, http://dx.doi.org/10.1039/C5TB02697K.
[21] N. Nombona, E. Antunes, W. Chidawanyika, P. Kleyi, Z. Tshentu, T. Nyokong, Synthesis, photophysics and photochemistry of phthalocyanine-ε- polylysine conjugates in the presence of metal nanoparticles against Staphylococcus aureus, J. Photochem. Photobiol. A Chem. 233 (2012) 24–33, http://dx.doi.org/10.1016/j.jphotochem.2012.02.012.
[22] C.S. Seney, B.M. Gutzman, R.H. Goddard, Correlation of size and surface-enhanced Raman scattering activity of optical and spectroscopic properties for silver nanoparticles, J. Phys. Chem. C 113 (2009) 74–80, http://dx.doi.org/10.1021/jp805698e.
[23] S. Hong, X. Li, Optimal size of Gold nanoparticles for surface-enhanced Raman spectroscopy under different conditions, J. Nanomater. 2013 (2013) 1–9, http://dx.doi.org/10.1155/2013/790323.
[24] L.A. Austin, M.A. MacKey, E.C. Dreaden, M.A. El-Sayed, The optical, photothermal, and facile surface chemical properties of gold and silver nanoparticles in biodiagnostics, therapy, and drug delivery, Arch. Toxicol. 88 (2014) 1391–1417, http://dx.doi.org/10.1007/s00204-014-1245-3.
[25] C.F. Bohren, D.R. Huffman, Absorption and Scattering of Light by Small Particles, Wiley, 1983.
[26] P.B. Johnson, R.W. Christy, Optical constants of the noble metals, Phys. Rev. B 6 (1972) 4370–4379.
[27] L.S. Jung, C.T. Campbell, T.M. Chinowsky, M.N. Mar, S.S. Yee, Quantitative interpretation of the response of surface plasmon resonance sensors to adsorbed films, Langmuir 14 (1998) 5636–5648, http://dx.doi.org/10.1021/la971228b.
[28] A. Arboleda, D. Miller, F. Cabot, M. Taneja, M.C. Aguilar, K. Alawa, G. Amescua, S.H. Yoo, J.-M. Parel, Assessment of Rose Bengal versus riboflavin photodynamic therapy for inhibition of fungal keratitis isolates, Am. J. Ophthalmol. 158 (2014) 64–70, http://dx.doi.org/10.1016/j.ajo.2014.04.007 e2.
[29] E.S. Keshishyan, Z.V. Zaporozhtseva, O.M. Zenina, V.S. Zrodnikov, Photodynamic Inactivation of Bacteria In Vitro Under the Effect of Blue Light, Bull. Exp. Biol. Med. 158 (2015) 475–477, http://dx.doi.org/10.1007/s10517-015-2788-x.
[30] T. Maisch, A. Eichner, A. Späth, A. Gollmer, B. König, J. Regensburger, W. Bäumler, Fast and effective photodynamic inactivation of multiresistant bacteria by cationic riboflavin derivatives, PLoS One 9 (2014) e111792, http://dx.doi.org/10.1371/journal.pone.0111792.
[31] R.W. Redmond, J.N. Gamlin, A Compilation of Singlet Oxygen Yields from Biologically Relevant Molecules, Photochem. Photobiol. 70 (1999) 391–475, http://dx.doi.org/10.1111/j.1751-1097.1999.tb08240.x.
[32] E. Amato, Y.A. Diaz-Fernandez, A. Taglietti, P. Pallavicini, L. Pasotti, L. Cucca, C. Milanese, P. Grisoli, C. Dacarro, J.M. Fernandez-Hechavarria, V. Necchi, Synthesis, characterization and antibacterial activity against gram positive and gram negative bacteria of biomimetically coated silver nanoparticles, Langmuir 27 (2011) 9165–9173, http://dx.doi.org/10.1021/la201200r.
[33] A. Taglietti, Y.A. Diaz Fernandez, E. Amato, L. Cucca, G. Dacarro, P. Grisoli, V. Necchi, P. Pallavicini, L. Pasotti, M. Patrini, Antibacterial Activity of Glutathione-Coated Silver Nanoparticles against Gram Positive and Gram Negative Bacteria, Langmuir 28 (2012) 8140–8148, http://dx.doi.org/10.1021/la3003838.
[34] R.P. Allaker, K. Memarzadeh, Nanoparticles and the control of oral infections, Int. J. Antimicrob. Agents 43 (2014) 95–104, http://dx.doi.org/10.1016/j.ijantimicag.2013.11.002.
[35] P. Dallas, V.K. Sharma, R. Zboril, Silver polymeric nanocomposites as advanced antimicrobial agents: Classification, synthetic paths, applications, and perspectives, Adv. Colloid Interface Sci. 166 (2011) 119–135, http://dx.doi.org/10.1016/j.cis.2011.05.008.
[36] P. Pallavicini, C.R. Arciola, F. Bertoglio, S. Curtosi, G. Dacarro, A. D'Agostino, F. Ferrari, D. Merli, C. Milanese, S. Rossi, A. Taglietti, M. Tenci, L. Visai, Silver nanoparticles synthesized and coated with pectin: An ideal compromise for antibacterial and anti-biofilm action combined with wound-healing properties, J. Colloid Interface Sci. 498 (2017) 271–281, http://dx.doi.org/10.1016/j.jcis.2017.03.062.
[37] K.R. Kasimova, M. Sadasivam, G. Landi, T. Sarna, M.R. Hamblin, Potentiation of photoinactivation of Gram-positive and Gram-negative bacteria mediated by six phenothiazinium dyes by addition of azide ion, Photochem. Photobiol. Sci. 13 (2014) 1541–1548, http://dx.doi.org/10.1039/c4pp00021h.
[38] M.N. Usacheva, M.C. Teichert, M.A. Biel, Comparison of the methylene blue and toluidine blue photobactericidal efficacy against gram-positive and gram-negative microorganisms, Lasers Surg. Med. 29 (2001) 165–173, http://dx.doi.org/10.1002/lsm.1105.
[39] P. Kaspler, S. Lazic, S. Forward, Y. Arenas, A. Mandel, L. Lilge, D. Casero, M. Pellegrini, O. Martínez-Maza, M.L. Penichet, S. Ferrari, G. Gasser, S.A. McFarland, A ruthenium(ii) based photosensitizer and transferrin complexes enhance photo-physical properties, cell uptake, and photodynamic therapy safety and efficacy, Photochem. Photobiol. Sci. 15 (2016) 481–495, http://dx.doi.org/10.1039/C5PP00450K.
[40] Y.-H. Choi, S.-H. Ko, S.J. Kim, W.-Y. Lee, J.H. Park, J.M. Lee, Induction of cell death by photodynamic therapy with a new synthetic photosensitizer DH-I-180-3 in undifferentiated and differentiated 3T3-L1 cells, Biochem. Biophys. Res. Commun. 337 (2005) 1059–1064, http://dx.doi.org/10.1016/j.bbrc.2005.09.151.
[41] D. Manoil, A. Filieri, J. Schrenzel, S. Bouillaguet, Rose bengal uptake by E. faecalis and F. nucleatum and light-mediated antibacterial activity measured by flow cytometry, J. Photochem. Photobiol. B Biol. 162 (2016) 258–265, http://dx.doi.org/10.1016/j.jphotobiol.2016.06.042.